Letter

Anisotropic magnetoresistance due to magnetization-dependent spin-orbit interactions

M. Q. Dong [1], Zhi-Xin Guo [1,*] and X. R. Wang [2,3,†]

[1] *State Key Laboratory for Mechanical Behavior of Materials, Center for Spintronics and Quantum System, School of Materials Science and Engineering, Xi'an Jiaotong University, Xi'an, Shaanxi 710049, China*

[2] *Physics Department, The Hong Kong University of Science and Technology, Clear Water Bay, Kowloon, Hong Kong*

[3] *HKUST Shenzhen Research Institute, Shenzhen 518057, China*

(Received 17 January 2023; accepted 22 June 2023; published 5 July 2023)

One of the recent surprising discoveries is the crystal-axis-dependent anisotropic magnetoresistance (CAMR) that depends on two magnetization components perpendicular to the current differently, in contrast to the conventional anisotropic magnetoresistance that predicts no change in resistance when the magnetization varies in the plane perpendicular to the current. Using density functional theory and Boltzmann transport equation calculations for bcc Fe, hcp Co, and bcc FeCo alloys, we show that CAMR can be accounted for by the magnetization-dependent spin-orbit interactions (SOI): Magnetization-dependent SOI modifies electron energy bands that, in turn, changes resistance. A phenomenological model reveals the intrinsic connection between SOI and order parameters. Such a mechanism is confirmed by the strong biaxial stain effect on CAMR. Our findings provide an efficient way of searching and optimizing materials with large CAMR, important in the design of high-performance spintronic devices.

DOI: 10.1103/PhysRevB.108.L020401

I. INTRODUCTION

The spin-dependent transport is a long-lasting topic in condensed matter physics [1]. The electrical conductivity of magnetic materials usually depends on its magnetization structures, resulting in various types of galvanomagnetic effects including newly discovered anomalous spin-Hall and its inverse effects [2]. Among them, anisotropic magnetoresistance (AMR) is a well-known phenomenon, which says that the longitudinal electrical resistivity depends only on the magnetization relative to the electric current [3–12]. The AMR is attributed to the relativistic spin-orbit interactions (SOI), which couple the electron orbital motions with their spins, and have a universal form in magnetic polycrystals: the change of longitudinal resistivity (or resistance) $\Delta\rho_{xx}(\alpha)$ follows $\Delta\rho_{xx}(\alpha) = \Delta\rho^0_{xx} cos^2\alpha$ with α being the angle between the magnetization and electric current [13].

Recently, an intrinsic crystal-axis-dependent anisotropic magnetoresistance (CAMR) effect has been discovered in FeCo alloy [14], where the electrical conductivity depends not only on the angle between current and magnetization, but also on the angle between the crystalline axis and magnetization [the angle between magnetization and z axis when the magnetization varies in the yz plane perpendicular to electric current flows, defined as the x direction, as shown in Fig. 1(d)]. Based on symmetry argument [15] and tensor analysis [16], a phenomenological magnetization dependence of electrical conductivity/resistivity [17], which gives rise to an intrinsic CAMR, was obtained. Nevertheless, microscopic mechanisms for the order-parameter-dependent CAMR are yet to be explored.

In this Letter, we use the density functional theory (DFT) and Boltzmann transport equations (BTE) on several magnetic single crystals, including bcc Fe, hcp Co, and bcc FeCo alloys, to investigate the microscopic origin of CAMR. For an electric current along [110] direction (denoted as x axis), we consider the magnetization along [$\bar{1}$10] (denoted as y axis) or along [001] direction (denoted as z axis). Whether longitudinal electronic resistance (ρ_{xx}) of these crystals varies with the magnetization direction in the yz plane or not depends on whether the SOI is included. Our calculations demonstrate that CAMR comes from the magnetization-dependent SOI. SOI leads to the energy band splitting near the Fermi level that, in turn, affects electronic transport. This intrinsic mechanism is confirmed by the strong biaxial strain dependence of CAMR.

II. METHOD

Our *ab initio* calculations are performed by using the QUANTUM ESPRESSO package based on the projector-augmented wave (PAW) method and a plane-wave basis set [18,19]. The exchange and correlation terms are described by a generalized gradient approximation (GGA) in the scheme of Perdew-Burke-Ernzerhof (PBE) parametrization, as implemented in the PSLIBRARY [20]. The energy accuracy is set as 1.0×10^{-8} Ry, and the energy cutoff is 180 Ry in all calculations. In the self-consistent field calculations, Monkhorst-Pack k meshes with a grid spacing of 0.025 Å^{-1} are adopted. Based on the DFT calculations, the maximally localized Wannier functions (MLWFs) [21–23] are then constructed by using WANNIER90 code [24,25], we construct a set of 18 MLWFs per atom using d_{xy}, d_{xz}, d_{yz}, and sp^3d^2 orbitals as first guesses.

*zxguo08@xjtu.edu.cn
†phxwan@ust.hk

Based on the MLWFs, the electronic conductivity can be calculated by employing the BTE method [26–29], where the chemical potential μ and temperature T dependence of electronic conductivity can be obtained by

$$\sigma_{ij}(\mu, T) = e^2 \int_{-\infty}^{+\infty} d\varepsilon \left(-\frac{\partial f(\varepsilon, \mu, T)}{\partial \varepsilon}\right) \Sigma_{ij}(\varepsilon), \quad (1)$$

where $f(\varepsilon, \mu, T)$ is the Fermi-Dirac distribution function

$$f(\varepsilon, \mu, T) = \frac{1}{e^{(\varepsilon-\mu)/k_B T} + 1} \quad (2)$$

and $\Sigma_{ij}(\varepsilon)$ is the transport distribution function tensor defined as

$$\Sigma_{ij}(\varepsilon) = \frac{1}{V} \sum_{n,\mathbf{k}} v_i(n, \mathbf{k}) v_j(n, \mathbf{k}) \tau(n, \mathbf{k}) \delta(\varepsilon - E_{n,\mathbf{k}}). \quad (3)$$

The sum in the above formulas is over all the energy bands (indexed by n) with all states $\mathbf{k}$ (including spin even if it is not explicitly denoted). $E_{n,\mathbf{k}}$ is the energy level and $v_i(n, \mathbf{k})$ is the ith component of group velocity of the nth band in state $\mathbf{k}$, δ is the Dirac's δ function, $V = N_k \Omega_c$ corresponds to the total volume of the system, and $\tau(n, \mathbf{k})$ is the relaxation time, which describes the average time interval between two consecutive collisions and is typically a complicated function of $\mathbf{k}$ and n. In our calculation, the relaxation time approximation is adopted [30,31], and the relaxation time is regarded as a constant, which is set as $\tau(n, \mathbf{k}) = 1.0 \times 10^{-14}$ s according to Ref. [32]. In addition, a dense $\mathbf{k}$ mesh of $200 \times 200 \times 200$ is employed to perform the Brillouin zone (BZ) integration for the electronic conductivity calculation. More details can be found in the Supplemental Material [33].

III. RESULT

We focus on the experimental setup in which the electric current is along [110] direction, and the electronic conductivity σ_{xx} or resistivity $\rho_{xx} = 1/\sigma_{xx}$ is calculated for magnetization along $[\bar{1}10]$ and [001] direction, respectively. The crystal structures of alloys and sample coordinates are shown in Fig. 1. As shown in Fig. S1 in Supplemental Material [33], the density of states (DOS) of Fe, Co, and FeCo all have significant splitting in spin-up and spin-down electrons near the Fermi level, which gives rise to sizable magnetic moments of the three materials. The calculated magnetic moments are $2.20\mu_B$/atom for bcc Fe and $1.62\mu_B$/atom for hcp Co, respectively. Whereas, in bcc FeCo, the magnetic moments are $2.53\,\mu_B$/atom for Fe and $1.68\,\mu_B$/atom for Co, respectively (Table S1).

We first explore the influence of magnetization direction on the electronic structures without a SOI. According to the Boltzmann formula presented in Sec. II, σ_{xx} relates only to the electron velocity along the x direction, which is the gradient of the band energy along Γ-X direction (the electron velocity can be evaluated as $v = dE/\hbar dk$, where E represents energy, k and $\hbar$ are the wave vector and the reduced Planck constant, respectively). Additional contributions from the wave vectors (or k points) outside the Γ-X direction, which have nonzero projection on Γ-X direction, also exist. Nevertheless, the band structure variation along Γ-X direction is expected to most directly reflect the change of σ_{xx}. As shown in

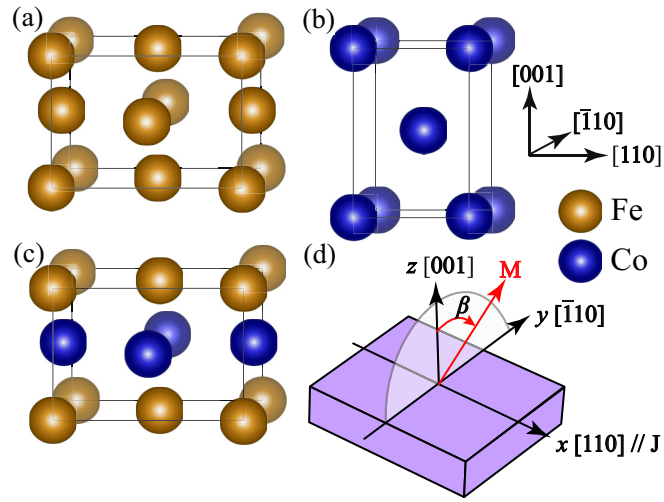

FIG. 1. Atomic structures of magnetic crystals (a)–(c) and the definition of angle β in the Cartesian coordinates (d). (a) bcc Fe (110), (b) hcp Co ($11\bar{2}0$), (c) bcc FeCo alloy (110), the brown and blue balls represent Fe and Co atoms, respectively. (d) Electric current is along [110] direction defined as x axis. $[\bar{1}10]$ and [001] are y and z axis, respectively. Magnetization $\mathbf{M}$ is in yz plane.

Figs. 2(a)–2(c), although the energy bands of spin-up and spin-down electrons significantly split along the electric current, they do not depend on the magnetization due to the collinear magnetic structure and the absence of a SOI. Electronic conductivity σ_{xx} [Eqs. (1)–(3)] is a function of electron velocity, Dirac's δ function, and electron relaxation time, where the first two quantities depend on the band structure while the last one does not, in relaxation time approximation (as discussed in Sec. II). Thus, the independence of band structure on magnetization direction means that no intrinsic CAMR exists in the absence of a SOI.

We discuss now the magnetization-dependent SOI, which affects band structure. Figures 2(d)–2(f) show the energy bands of different magnetizations with a SOI. It is clear that the SOI induces band split in all three magnetic crystals. Notably, the band split strongly depends on the magnetization direction, and bands are different when it is along [001] and $[\bar{1}10]$ directions. Particularly, the split becomes prominent for the intersected bands around certain $\mathbf{k}$ points. Since the change of band structure leads to the change of electron velocity and thus σ_{xx}, this result shows that the magnetization-dependent split of energy bands induced by the SOI is responsible for the intrinsic CAMR. Band splitting may not be the sole cause of CAMR and there may be other mechanisms responsible for CAMR (yet to be explored). However, in the BTE calculations, the band structure merely determines the electronic conductance under the relaxation time approximation [see Eqs. (1)–(3)]. Thus, these results show that the intrinsic CAMR originates from the magnetization-dependent split of energy bands induced by the SOI. Dominant band split occurs in certain energy range, [0.15 eV, 0.35 eV] for bcc Fe (110) and bcc FeCo (110), and [−0.40 eV, −0.25 eV] for hcp Co ($11\bar{2}0$) [marked by the grey circles in Figs. 2(d)–2(f)], which depends on the

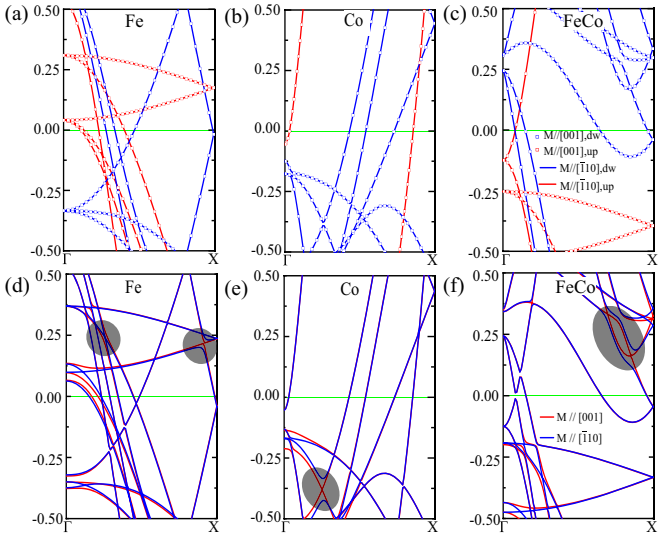

FIG. 2. Calculated energy bands without/with the SOI for bcc Fe (110), hcp Co (11$\bar{2}$0), and bcc FeCo (110) alloy when the magnetization is along [001] direction or [$\bar{1}$10] direction, respectively. (a)–(c) Energy bands of the spin projection when the magnetization is along [001] direction and [$\bar{1}$10] direction without the SOI. The red and blue small squares are the energy bands of spin-up and spin-down electrons with the magnetization along [001] direction, respectively. The red and blue solid lines are the energy bands of spin-up and spin-down electrons with the magnetization is along [$\bar{1}$10], respectively. The solid lines and small squares completely coincide, showing the independence of energy bands on the magnetization direction without the SOI. (d)–(f) Energy bands with the SOI. Red and blue lines represent the energy bands of magnetization along the [001] and [$\bar{1}$10] directions, respectively. Note that the energy bands of spin-up and spin-down electrons are not distinguished in the SOI calculations. The split of energy bands induced by different magnetization direction are indicated by the grey circles. The Γ-X direction in the BZ corresponds to the x axis in the real space.

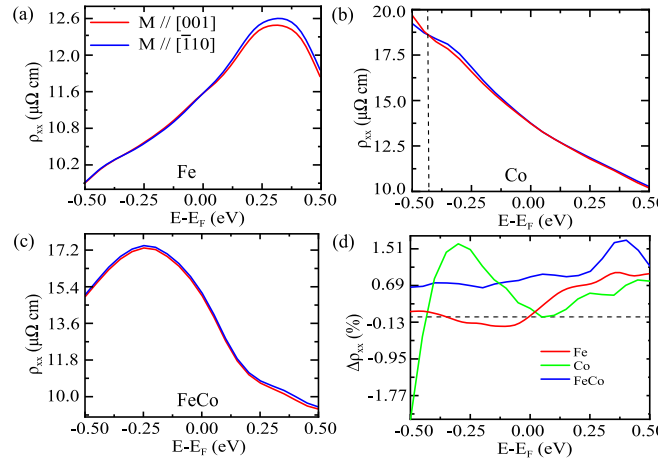

FIG. 3. The Fermi-level dependences of resistivity for (a) bcc Fe (110), (b) hcp Co (11$\bar{2}$0), and (c) bcc FeCo (110) alloy, when the magnetization is along [001] (the red) and [$\bar{1}$10] (the blue), respectively. (d) The Fermi-level dependences of $\Delta\rho_{xx}$ of three alloys. The black dashed lines in (b) and (d) indicate $\rho_{xx}^{\bar{1}10} = \rho_{xx}^{001}$.

crystal structures. This feature indicates that the bcc and hcp structures have distinct CAMR behaviors.

To confirm above analysis, we calculate the electrical resistivity of the three magnetic crystals in the presence of the SOI. Figures 3(a)–3(c) show how ρ_{xx} changes when the Fermi level is tuned (relative to undoped crystal Fermi energy E_F) while the magnetization aligns along [001] and [$\bar{1}$10], respectively. It is found that ρ_{xx} near E_F for all three materials are in the range of 11–15 $\mu\Omega$ cm, agree well with the experimental values of around 10.8 $\mu\Omega$ cm [14]. Moreover, ρ_{xx} of different magnetization directions differs from each other slightly, and the variations have obvious energy dependence in all three magnetic crystals. Significant difference of ρ_{xx} for magnetization along y and z axis occur concurrently with sizable SOI induced band split. $\Delta\rho_{xx} = (\rho_{xx}^{\bar{1}10} - \rho_{xx}^{001})/\rho_{xx}^{001} \times 100\%$ clearly reveals the phenomenon. $\rho_{xx}^{\bar{1}10}$ and ρ_{xx}^{001} denote the electrical resistivity when the magnetization are along [$\bar{1}$10] and [001], respectively. As shown in Fig. 3(d), the maximum value of $\Delta\rho_{xx}$ in both bcc Fe (1.0%) and bcc FeCo (1.6%) appears around 0.37 eV above E_F, whereas $\Delta\rho_{xx}$ becomes the maximum around 0.3 eV below E_F for hcp Co (1.6%). A common feature is that all the maximum value of $\Delta\rho_{xx}$ is 1.0%–1.6%, indicating the robustness of CAMR value, which hardly depends on the component of Fe/Co in the FeCo alloy. The calculated $\Delta\rho_{xx}$ is in good agreement with the experimental value (1.0%) [14], showing the reliability of BTE method for the CAMR. The energy levels with the maximum $\Delta\rho_{xx}$ locate exactly in the energy range with the most significant band splits [Figs. 2(d)–2(f)]. These results clearly show that the intrinsic CAMR originates from magnetization-dependent split of energy bands induced by the SOI.

We use FeCo to further explore the relationship between the anisotropic magnetoresistance and strength of the SOI. Figure 4(a) shows how ρ_{xx} of FeCo significantly varies with the angle β. It can be well fitted by a sine function, which exhibits a twofold symmetry. This result is in good agreement with experimental observations in Ref. [14]. The β dependence of the SOI strength can be obtained from averaging E_{SOI} [34] over the electronic states

$$E_{SOI} = \frac{1}{c^2}\frac{1}{r}\frac{dV}{dr} l \cdot s, \tag{4}$$

where c is the speed of light, r is the radial distance of the electron from the center of its atom, V is the effective potential on the electron, and l, s are orbital angular momentum and

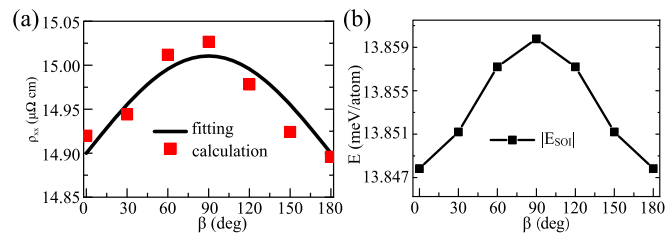

FIG. 4. (a). Calculated ρ_{xx} of FeCo at $E_F - 0.5$ eV as a function of β, the red dot is the calculation, and the black solid line is the result after fitting with sine function. (b). The variations of $|E_{SOI}|$ of FeCo with β.

spin operators, respectively. As shown in Fig. 4(b), $|E_{SOI}|$ is also a sine function of β, similar to that of the ρ_{xx}. The feature confirms that the SOI is responsible for the CAMR.

We additionally investigate the relationship between the SOI and magnetocrystalline anisotropy. As shown in Fig. S3 in Supplemental Material, the magnetization-direction-dependent magnetic anisotropic energy (MAE) of FeCo is zero without a SOI. The result indicates that the electron hopping can hardly be influenced by the magnetization. Then we explore the variation of MAE with β under the SOI effect. As shown in Fig. S3, the variation of MAE exhibits a sine function on β, in agreement with the assertion that the SOI is the origin of both intrinsic CAMR and the MAE in a collinear magnetization magnetic material.

Furthermore, we calculate the magnetic moments without (Table S1) and with (Table S2) the SOI. It is found that similar to the results obtained without the SOI, the magnitude of magnetic moments does not depend on the magnetization directions in the presence of the SOI. This result excludes the contribution from variation of magnitude of magnetic moments to CAMR in our studied system.

We consider now the intrinsic connection of the SOI to order parameters such as the magnetization and crystalline axis. According to the general form [35], the SOI of a conduction electron can be expressed as

$$H_{SOI} = \frac{\hbar e}{2mc^2}(\vec{\sigma} \times \vec{\nabla} U) \cdot \vec{v}_c, \tag{5}$$

where U is the electrical potential and $\vec{\nabla} U$ corresponds to effective electrical field, $\vec{\sigma}$ is the spin, and $\vec{v}_c$ is the velocity of conduction electrons influenced by the external electrical field. Considering that the spin polarization of most conduction electrons in a magnetic metal is parallel to the magnetization direction $\vec{M}$, the magnetization-dependent SOI for the conduction electrons can be further obtained

$$H^M_{SOI} = \frac{\alpha \hbar e}{2mc^2}(\vec{M} \times \vec{\nabla} U) \cdot \vec{v}_c \tag{6}$$

by defining $\vec{\sigma} = \alpha \vec{M}$, where α is a coefficient. Equation (6) works only for the conduction electrons with $\vec{\sigma} // \vec{M}$.

As discussed in the Supplemental Material of Ref. [36], $\vec{\nabla} U$ strongly depends on the spin-polarized charge density (SPCD) in the magnetic crystal. Considering that the majority-spin (denoted as $\uparrow$) electrons are in charge of the electronic conductivity, one can focus on SOI for the $\uparrow$ spin, where the effective electrical field can be expressed as $\vec{\nabla} U^{\uparrow}(r) \propto n^{\uparrow}(r) \vec{\nabla} n^{\uparrow}(r)$ with $n^{\uparrow}(r)$ and $\vec{\nabla} n^{\uparrow}(r)$ being the SPCD and its gradient at position $\vec{r}$ for the $\uparrow$ electrons, respectively [36]. Hence, it is obvious that different $\vec{\nabla} U^{\uparrow}(r)$ values would be obtained if $n^{\uparrow}(r)$ and $\vec{\nabla} n^{\uparrow}(r)$ are anisotropic, which are true in general. Although bcc Fe is highly symmetric, its $n^{\uparrow}(r)$ [$\vec{\nabla} n^{\uparrow}(r)$] along [$\bar{1}$10] and [001] directions are still distinct according to the symmetry analysis, which results in $\nabla_{\bar{1}10} U^{\uparrow} \neq \nabla_{001} U^{\uparrow}$. According to Eq. (6), the variation of SOI$'s$ strength is attributed by $\vec{M} \times \vec{\nabla} U$ when $\vec{v}_c$ is fixed, where the strongest SOI corresponds to the case $\vec{M} \perp \vec{\nabla} U$. Therefore, although the magnetization is perpendicular to the electric current (along [110] direction) in both cases of $\vec{M}//$[001] and $\vec{M}//$[$\bar{1}$10], different SOI strength can be still induced by the fact that $\nabla_{\bar{1}10} U^{\uparrow} \neq \nabla_{001} U^{\uparrow}$. This mechanism should be general and applicable to hcp Co, and bcc FeCo.

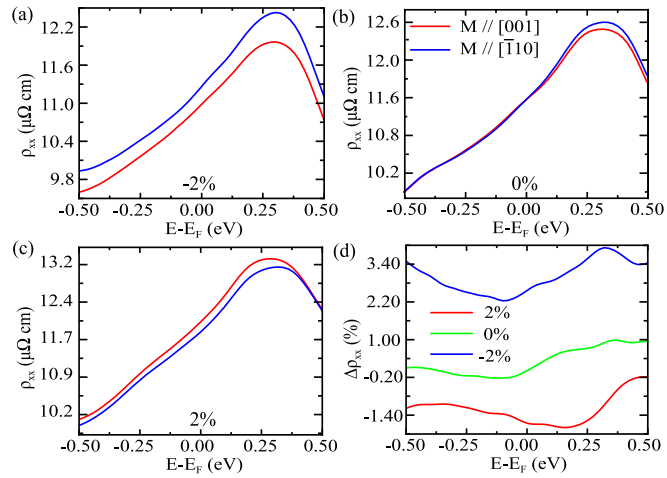

FIG. 5. (a) Resistivity of bcc Fe (110) corresponding to different magnetization directions at strain of -2% and 2%. Red (blue) solid and dashed lines represent the ρ_{xx} when the magnetization along the [110] ([$\bar{1}$10]) direction, and the strain is applied at 2% and -2%, respectively. (b) $\Delta\rho_{xx}$ of Fe (110) varying with the position of Fermi energy under different strains.

The above results clearly reveal the intrinsic correlation among magnetization (corresponds to $\vec{M}$), crystalline axis (corresponds to $\vec{\nabla} U$), and external electrical field (corresponds to $\vec{v}_c$). The coupling between order parameters, i.e., magnetization and crystal axis, leads to the magnetization-dependent SOI and thus CAMR. This mechanism is different from the one in conventional AMR, which solely comes from the coupling between magnetization and external electrical field (or electric current) and ignores the crystalline-axis dependence of $\vec{\nabla} U$ [6,37,38].

To confirm above results, we further investigate the biaxially strain-dependent CAMR. The biaxial strain is expected to change the anisotropy of SPCD and thus the difference between $\nabla_{\bar{1}10} U^{\uparrow} \neq \nabla_{001} U^{\uparrow}$, which results in significant variation of CAMR. Figure 5(a) shows the energy level (relative to E_F) dependence of ρ_{xx} of bcc Fe with the magnetization along [001] and [$\bar{1}$10] at different strains, respectively. It is found that the compressive and tensile strains have completely different effect on ρ_{xx}, which leads to the divergence of CAMR. When a compressive strain (-2%) is applied, ρ_{xx} with magnetization along [$\bar{1}$10] is significantly larger than that along [001] in the whole energy region near E_F. Whereas it has a converse behavior when a tensile strain (2%) is applied. The corresponding $\Delta\rho_{xx}$ is additionally shown in Fig. 5(b). As one can see, strain can significantly enhance CAMR, the maximum $|\Delta\rho_{xx}|$ reaches 4.0 and 1.6 times larger than that without strain (1.0%) under the compressive and tensile strains, respectively. This result confirms the intrinsic coupling between magnetization and crystalline lattice, which gives rise to the magnetization-dependent SOI and thus CAMR.

Before conclusion, it should be pointed out that CAMR originating from the coupling between interfacial field and magnetization in bilayer materials has been recently proposed

[39]. The present CAMR theory is for the homogeneous materials, not for bilayers.

IV. CONCLUSION

In summary, CAMR in Fe, Co, and FeCo alloy originates from the magnetization-dependent SOI. Using the DFT calculations and BTE, we show that the SOI splits intersecting energy bands around the Fermi level. Different magnetization direction gives rise to different SOIs that, in turn, lead to different resistivity, or CAMR. This is an intrinsic CAMR. SOI is essential in CAMR since the energy bands do not depend on magnetization direction in the absence of the SOI. A phenomenological model that reveals the relationship between SOI and order parameters (magnetization and crystalline lattice) is proposed and is confirmed by the strong strain dependence of CAMR.

ACKNOWLEDGMENTS

We acknowledge financial support from the Natural Science Foundation of China (Grants No. 12074301, No. 11974296), and Hong Kong RGC (Grants No. 16300522, No. 16302321, and No. 16301619). We gratefully acknowledge the computational resources provided by the HPCC platform of Xi′an Jiaotong University.

[1] C. Chappert, A. Fert, and F. N. Van Dau, The emergence of spin electronics in data storage, Nature Mater. **6**, 813 (2007).

[2] X. R. Wang, Anomalous spin Hall and inverse spin Hall effects in magnetic systems, Commun. Phys. **4**, 55 (2021).

[3] W. Döring, Die Abhängigkeit Des Widerstandes von Nickelkristallen von der Richtung der spontanen Magnetisierung, Ann. Phys. (NY) **424**, 259 (1938).

[4] T. McGuire and R. Potter, Anisotropic magnetoresistance in ferromagnetic 3d alloys, IEEE Trans. Magn. **11**, 1018 (1975).

[5] L. Berger, Influence of spin-orbit interaction on the transport processes in ferromagnetic nickel alloys, in the presence of a degeneracy of the 3d band, Physica **30**, 1141 (1964).

[6] I. A. Campbell, A. Fert, and O. Jaoul, The spontaneous resistivity anisotropy in Ni-based alloys, J. Phys. C: Solid State Phys. **3**, S95 (1970).

[7] K. M. Seemann, F. Freimuth, H. Zhang, S. Blügel, Y. Mokrousov, D. E. Bürgler, and C. M. Schneider, Origin of the planar Hall effect in nanocrystalline $Co_{60}Fe_{20}B_{20}$, Phys. Rev. Lett. **107**, 086603 (2011).

[8] L. Nádvorník, M. Borchert, L. Brandt, R. Schlitz, K. A. de Mare, K. Výborný, I. Mertig, G. Jakob, M. Kläui, S. T. B. Goennenwein, M. Wolf, G. Woltersdorf, and T. Kampfrath, Broadband Terahertz Probes of Anisotropic Magnetoresistance Disentangle Extrinsic and Intrinsic Contributions, Phys. Rev. X **11**, 021030 (2021).

[9] R. Tomar, S. Kakkar, C. Bera, and S. Chakraverty, Anisotropic magnetoresistance and planar Hall effect in (001) and (111) $LaVO_3/SrTiO_3$ heterostructures, Phys. Rev. B **103**, 115407 (2021).

[10] Y. Miao, D. Yang, L. Jia, X. Li, S. Yang, C. Gao, and D. Xue, Magnetocrystalline anisotropy correlated negative anisotropic magnetoresistance in epitaxial $Fe_{30}Co_{70}$ thin films, Appl. Phys. Lett. **118**, 042404 (2021).

[11] P. Ritzinger, H. Reichlova, D. Kriegner, A. Markou, R. Schlitz, M. Lammel, D. Scheffler, G. H. Park, A. Thomas, P. Středa, C. Felser, S. T. B. Goennenwein, and K. Výborný, Anisotropic magnetothermal transport in Co_2MnGa thin films, Phys. Rev. B **104**, 094406 (2021).

[12] F. Zeng, C. Zhou, M. Jia, D. Shi, Y. Huo, W. Zhang, and Y. Wu, Strong current-direction dependence of anisotropic magnetoresistance in single crystalline Fe/GaAs(110) films, J. Magn. Magn. Mater. **499**, 166204 (2020).

[13] D. Thompson, L. Romankiw, and A. Mayadas, Thin film magnetoresistors in memory, storage, and related applications, IEEE Trans. Magn. **11**, 1039 (1975).

[14] F. L. Zeng, Z. Y. Ren, Y. Li, J. Y. Zeng, M. W. Jia, J. Miao, A. Hoffmann, W. Zhang, Y. Z. Wu, and Z. Yuan, Intrinsic mechanism for anisotropic magnetoresistance and experimental confirmation in Co_xFe_{1-x} single-crystal films, Phys. Rev. Lett. **125**, 097201 (2020).

[15] E. De Ranieri, A. W. Rushforth, K. Výborný, U. Rana, E. Ahmad, R. P. Campion, C. T. Foxon, B. L. Gallagher, A. C. Irvine, J. Wunderlich, and T. Jungwirth, Lithographically and electrically controlled strain effects on anisotropic magnetoresistance in (Ga,Mn)As, New J. Phys. **10**, 065003 (2008).

[16] Y. Zhang, X. R. Wang, and H. W. Zhang, Extraordinary galvanomagnetic effects in polycrystalline magnetic films, Europhys. Lett. **113**, 47003 (2016).

[17] X. R. Wang, A theory for anisotropic magnetoresistance in materials with two vector order parameters, Chin. Phys. Lett. **39**, 027301 (2022).

[18] P. Giannozzi, S. Baroni, N. Bonini, M. Calandra, R. Car, C. Cavazzoni, D. Ceresoli, G. L. Chiarotti, M. Cococcioni, I. Dabo, A. Dal Corso, S. de Gironcoli, S. Fabris, G. Fratesi, R. Gebauer, U. Gerstmann, C. Gougoussis, A. Kokalj, M. Lazzeri, L. Martin-Samos *et al.*, QUANTUM ESPRESSO: A modular and open-source software project for quantum simulations of materials, J. Phys.: Condens. Matter **21**, 395502 (2009).

[19] P. Giannozzi, O. Andreussi, T. Brumme, O. Bunau, M. Buongiorno Nardelli, M. Calandra, R. Car, C. Cavazzoni, D. Ceresoli, M. Cococcioni, N. Colonna, I. Carnimeo, A. Dal Corso, S. de Gironcoli, P. Delugas, R. A. DiStasio, A. Ferretti, A. Floris, G. Fratesi, G. Fugallo *et al.*, Advanced capabilities for materials modelling with QUANTUM ESPRESSO, J. Phys.: Condens. Matter **29**, 465901 (2017).

[20] A. Dal Corso, Pseudopotentials periodic table: From H to Pu, Comput. Mater. Sci. **95**, 337 (2014).

[21] G. H. Wannier, The structure of electronic excitation levels in insulating crystals, Phys. Rev. **52**, 191 (1937).

[22] N. Marzari, A. A. Mostofi, J. R. Yates, I. Souza, and D. Vanderbilt, Maximally localized Wannier functions: Theory and applications, Rev. Mod. Phys. **84**, 1419 (2012).

[23] N. Marzari and D. Vanderbilt, Maximally localized generalized Wannier functions for composite energy bands, Phys. Rev. B **56**, 12847 (1997).

[24] A. A. Mostofi, J. R. Yates, Y.-S. Lee, I. Souza, D. Vanderbilt, and N. Marzari, Wannier90: A tool for obtaining maximally-localised Wannier functions, Comput. Phys. Commun. **178**, 685 (2008).

[25] G. Pizzi, V. Vitale, R. Arita, S. Blügel, F. Freimuth, G. Géranton, M. Gibertini, D. Gresch, C. Johnson, T. Koretsune, J. Ibañez-Azpiroz, H. Lee, J.-M. Lihm, D. Marchand, A. Marrazzo, Y. Mokrousov, J. I. Mustafa, Y. Nohara, Y. Nomura, L. Paulatto *et al.*, Wannier90 as a community code: New features and applications, J. Phys.: Condens. Matter **32**, 165902 (2020).

[26] J. M. Ziman, *Principles of the Theory of Solids*, 2nd ed. (Cambridge University Press, Cambridge, 1972).

[27] G. Grosso and G. P. Parravicini, *Solid State Physics*, 2nd ed. (Academic Press, Amsterdam, 2014).

[28] G. D. Mahan, Transport Properties, in *International Tables for Crystallography*, Vol. D (Kluwer, Dordrecht, 2006), Chap. 1.8, pp. 220–227.

[29] G. Pizzi, D. Volja, B. Kozinsky, M. Fornari, and N. Marzari, BoltzWann: A code for the evaluation of thermoelectric and electronic transport properties with a maximally-localized Wannier functions basis, Comput. Phys. Commun. **185**, 422 (2014).

[30] T. J. Scheidemantel, C. Ambrosch-Draxl, T. Thonhauser, J. V. Badding, and J. O. Sofo, Transport coefficients from first-principles calculations, Phys. Rev. B **68**, 125210 (2003).

[31] G. K. H. Madsen, Automated search for new thermoelectric materials: The case of LiZnSb, J. Am. Chem. Soc. **128**, 12140 (2006).

[32] T. L. Monchesky, A. Enders, R. Urban, K. Myrtle, B. Heinrich, X.-G. Zhang, W. H. Butler, and J. Kirschner, Spin-dependent transport in Fe and Fe/Au multilayers, Phys. Rev. B **71**, 214440 (2005).

[33] See Supplemental Material at http://link.aps.org/supplemental/10.1103/PhysRevB.108.L020401 for the magnetic moments and density of states (DOS) for Fe, Co, and FeCo; details of generating the maximized localized Wannier function (MLWF); details of calculating Boltzmann transport equations (BTE); the relationship between SOI and magnetocrystalline anisotropy.

[34] K. Yamauchi and S. Picozzi, Orbital degrees of freedom as origin of magnetoelectric coupling in magnetite, Phys. Rev. B **85**, 085131 (2012).

[35] N. Nagaosa, J. Sinova, S. Onoda, A. H. MacDonald, and N. P. Ong, Anomalous Hall effect, Rev. Mod. Phys. **82**, 1539 (2010).

[36] P. Li, J.-Z. Zhang, Z.-X. Guo, T. Min, and X. Wang, Intrinsic anomalous spin Hall effect, Sci. China Phys. Mech. Astron. **66**, 227511 (2023).

[37] S. Kokado, M. Tsunoda, K. Harigaya, and A. Sakuma, Anisotropic magnetoresistance effects in Fe, Co, Ni, Fe_4N, and half-metallic ferromagnet: A systematic analysis, J. Phys. Soc. Jpn. **81**, 024705 (2012).

[38] S. Kokado and M. Tsunoda, Anisotropic magnetoresistance effect: General expression of AMR ratio and intuitive explanation for sign of AMR ratio, in *Advanced Engineering Materials III, Advanced Materials Research*, Vol. 750 (Trans Tech Publications Ltd, 2013), pp. 978–982.

[39] X. R. Wang, C. Wang, and X. S. Wang, A theory of unusual anisotropic magnetoresistance in bilayer heterostructures, Sci. Rep. **13**, 309 (2023).